CHAPTER 4: Thermodynamic and Nucleation Rate of Gadolinium Oxide Nanoclusters

4.1 Introduction

Nucleation is a fundamental step during forming molecular-sized nuclei from prenucleation clusters either by supersaturation or high temperature mediated solid-state reactions. [372] This nucleation involved the crystal formation and growth at standard and higher temperature points. [373] Understanding kinetic and thermodynamic barriers is crucial to gain in-depth insight into nucleation pathways. [372] Subsequently, the current research is focused on calculating nucleation rates with the help of kinetic and thermodynamic barriers during solid reactions at high temperatures. As the nucleation rate is a product of two terms, the first is a kinetic barrier (J_k=A_a exp (E_a./RT)), and the second is a thermodynamic barrier (exp BG/RT), where E_a. (activation energy of nucleation), ΔG (thermodynamic barrier of nucleation) and T (temperature) are the main parameters in kinetic and thermodynamic terms. [372] Furthermore, till now, during nucleation rate computation, the accuracy in the calculated value of J_k is not much investigated, and many scientific research communities have assumed J_k as a constant term. [372] For example, the formula for J_k computation was given as D/5d, Where D and dare diffusion coefficient and average diameter of monomers. [372]

On the contrary, the atomic force microscope (AFM) technique was adopted for J_k computation at room temperature. [374] For instance, the calculated value of J_k for the nucleation of silica on the two different substrates of NH_3/COO- and carboxyl mixed hybrid were $10^{14.8}$ and $10^{13.5}$ (nuclei m^{-2} min^{-1}), respectively. [268] However, for different nucleation studies, such techniques for J_k calculation are still lacking, and accurate computation of J_k at high temperatures is still absent. The nucleation and growth kinetic computations are frequently neglected due to the complexity of the calculation of reaction rate and microscopic approximations. [375] Therefore, in the current research, the kinetic

barrier of nucleation (J_k) is computed precisely by keeping the accuracy in the calculated value of apparent activation energy of nucleation (E_a) and pre-exponential kinetic factor (A_a) at high temperatures. Accurate iso-conversational techniques were adopted to compute A_a and E_a precisely at high temperatures using non-isothermal TGA mass loss data. To date, the crystallization of the InSe system has been investigated in the high-temperature range (40 °C-550 °C) by adopting iso-conversational techniques using TGA technology. [376] The nucleation of calcite crystal was investigated at 315 °C, and their apparent activation energy of dehydration was computed. [377] Despite the observation of nucleation rate of ultra-small osmium clusters to ultra-small nanocrystals [273] in a narrow temperature range from 20 °C to 100 °C and InSe crystallization-based nucleation in a high-temperature range (40 °C-550 °C). [378] The kinetic barrier of nucleation (J_k), thermodynamic parameters and dependent nucleation rate (J_n) accurate computations are still absent. Thus, the accurate the calculation of apparent activation energy of nucleation (kinetic determination) of inorganic nanomaterials is urgently required for calculation of nucleation rate accurately at high temperature.

Over the decades, the kinetic investigation of inorganic materials was focused on investigating their solid and gaseous products. In the current situation, various well-defined models were proposed by many scientific communities to precisely calculate apparent activation energy. [379] Firstly, Inorganic material was kept in a TGA machine, and its mass loss data with time and temperature were collected, and then its corresponding activation energy of nucleation i.e., is obtained through the Vyazovkin advance iso-conversional approach (V.AIC) technique. [380] Different conversion-based iso-conversional models were proposed by many scientific communities like Tang, Starink, and KAS, methods for computation of apparent activation energy, but the above methods are purely governed by approximations. On the other hand, In the Vyazovkin technique,

the average of apparent activation energy values 0 to α is often observed. Thus, the Vyazovkin AIC technique was adopted to remove any type of approximation, and this technique eliminates averaging of calculated apparent activation energy. Subsequently, Vyazovkin AIC eliminates any type of systematic error over a range of Bα compared to the KAS, Tang, Starink, and Vyazovkin technique. The Vyazovkin AIC technique is used in current research for computation of apparent activation energy of nucleation and consequently dependent kinetic barrier of nucleation against conversion. In the current research, the accuracy in the calculation of J_k has been enhanced automatically through the Vyazovkin AIC technique by keeping $\Delta\alpha$ so small (~0.005).

The trivalent rare earth elements exhibit the most stable oxide due to their occupied 4f subshell electron, [312] which opens their application in medical diagnosis and biochemical probes. [323] The thermodynamically stable gadolinium oxide (Gd_2O_3) is an up-and-coming candidate for optoelectronics, [322] nanoelectronics, biosensing, [381] and photocatalytic activity [354] due to their high band gap (5.32 eV) and high dielectric constant (K=16). [382] However, the promising proton relaxation properties of Gd_2O_3 nanomaterials opens the door for MR imaging modality, [358] hence the development of sub nano size (< 2 nm) Gd_2O_3 nanomaterials is very much needed to enhance the proton relaxation [306] and easy removal from the body draw the considerable attention toward low temperature directed synthesis of Gd_2O_3 nanoclusters.

The synthesis of Gd_2O_3 in sub nano size in a different approach has been reported, for example, S V Mahajan et al. synthesized 3 nm size Gd_2O_3: RE (RE: Rare Earth) nanoparticles using thermal decomposition of rare earth directed oleate compound, [318] Cao et al. demonstrated the synthesis of square shaped Gd_2O_3 through thermal decomposition method of Oleic and rare earth complex at very high temperature of 320 °C/min. [56] Shafqat et al. synthesize ultra-small (5.2 nm) undoped (Gd_2O_3) and doped

(RE^{+3}: Gd_2O_3) crystals using benzyl alcohol as a reaction solvent through a rapid microwave-assisted route. [312] Lee et al. demonstrated the synthesis of paramagnetic Gd_2O_3 nanoparticles using Gd^{+3} salt precursor under continuous oxygen flow for 24 hrs. in tripropylene glycol as a reaction solvent. [383] In most of the above reports, the main focus is to obtain uniform homogeneous nanomaterial with a high degree of repeatability, which depends on the nucleation rate and stability of the nanomaterial. However, these nanomaterials kinetics and thermodynamics parameters could be very well explained through mathematical calculation. [384] [385] Hence, thermally stable material plays a decisive role in limiting material application. [386] To the best of our knowledge, till now, there is no literature to evaluate the thermodynamic parameter, nucleation rate, and interfacial energy of prepared Gd_2O_3 nanoclusters. We exclusively synthesize these nanoclusters for this objective using the wet chemical method. The weak reducing agent L-Ascorbic is used for the synthesis of the nanocluster, and bovine serum albumin (BSA) is used for stabilizing the nanocluster as a capping agent because BSA is a well-known stabilizing agent with high biocompatibility to the nanomaterials gives the promising protein template for the synthesis of Gd_2O_3 nanoclusters.

The Thermogravimetric analysis was used to evaluate the thermal behavior of Gd_2O_3 nanoclusters. The Starink, [257] Tang, [387] FWO, (Flynn Wall Ozawa), [388] KAS (Kissinger Akahira Sunose), [389] Vyazovkin, [259] and Vyazovkin AIC [390] models were utilized to calculate the activation energy (E_a). However, the most accurate and reliable Vyazovkin AIC model was used to predict the random nucleation within Gd_2O_3 nanoclusters at very high temperatures to compute the value of activation energy and frequency factor (A_a). The thermodynamic boundary and kinetics of the nanoclusters disrupting after initiation of the nucleation process, hence interfacial energy, nucleation rate, and thermodynamic parameter like ΔH, ΔS, and ΔG were examined at three

temperature ranges of 10 °C/min, 15 °C/min and 20 °C/min under inert nitrogen atmosphere, which is a function of conversion reaction and specific reaction.

4.2 Computation and theoretical background with determination kinetics parameters

4.2.1 Thermogravimetric Analysis (TGA)

Thermal stability and kinetics parameters through thermogravimetric analysis on gadolinium oxide nanoclusters (Gd_2O_3 NCs) powder were archived at different heating rates of 10 °C/min, 15 °C/min, and 20 °C/min between the heating range of 27 °C/min to 689 °C/min under the continuous nitrogen atmosphere with the flow of 20 ml/min. [391] The mathematical model of free iso-conversion methods was used to calculate the transformative activation energy at each unique conversion point. Additionally, the *Z (α)* master plot, which is the mechanism of thermal degradation of Gd_2O_3 NCs, was evaluated by plotting the *Z (α)* vs. conversion (*α)*, Where *Z (α)* is the product of integral function *I (α)* and differential function *f (α)*. The data from the experimental curve plot shows the third order nucleation (Figure 4.3), further identifying the mechanism of reaction at all three-heating rates of 10 °C/min, 15 °C/min, and 20 °C/min.

4.2.2 Kinetics Parameter

The thermal degradation reaction of Gd_2O_3 NCs can be elaborate by Equation (1) and Equation (2), with the function of conversion (α) and time (t). [374]

$$\frac{d\alpha}{dt} = K(T).f(\alpha) \ldots\ldots\ldots\ldots\ldots\ldots\ldots\ldots\ldots\ldots \text{(1)}$$

$$\left[\alpha = \left[\frac{M_o - M_t}{M_0 - M_f}\right]\right] \ldots\ldots\ldots\ldots\ldots\ldots\ldots\ldots\ldots\ldots \text{(2)}$$

Where $K\ (T)$ Temperature-dependent constant and t is reaction time. $f(\alpha)$ is a different function for change in a reaction rate constant at a particular conversion *(α)*. M_o, M_f and M_t are weights of Gd_2O_3 NCs for the initial, final, and at a particular time (t).

The disintegration rate of any solid /powder can be well described by the Arrhenius equation, which can illustrate the interrelation between reaction rate constant and temperature Equation (3). [392][393]

$$\frac{d\alpha}{dt} = Ae^{\frac{E_a}{RT}}.f\ (\alpha) \ldots\ldots\ldots\ldots\ldots\ldots (3)$$

Where A_a is the pre-exponential factor, E_a is activation energy (Arrhenius). R is the universal gas constant, and *f (α)* is a deferential function at each conversion point (α).

Further disintegration rate at a constant heating rate (β) of reaction was described by transferring the Arrhenius equation (Equation 3) into the non-isothermal rate equation (Equation 4), which is a function of temperature.

$$\frac{d\alpha}{dt} = \frac{A}{\beta}e^{\frac{E_a}{RT}}.f\ (\alpha) \ldots\ldots\ldots\ldots\ldots\ldots (4)$$

Where β is the constant heating rate.

Now the integration of Equation (4) from limit 0 to α

$$\int_0^{\alpha} \frac{d\alpha}{f\alpha} = \int_{T_i}^{T} \frac{A}{\beta} e^{\left(-\frac{E_a}{RT}\right)}.dT \ldots\ldots\ldots\ldots\ldots\ldots (5)$$

$$I(\alpha) = \frac{A}{\beta} \int_{T_i}^{T} e^{\left(-\frac{E_a}{RT}\right)}.dT \ldots\ldots\ldots\ldots\ldots\ldots (6)$$

So, rearrangement for Equation (5) and Equation (6) represents as

$$\int_0^{\alpha} \frac{d\alpha}{f\alpha} = I(\alpha) = \frac{A}{\beta} \int_{T_i}^{T} e^{\left(-\frac{E_a}{RT}\right)}.dT \ldots\ldots\ldots\ldots (7)$$

Where T_i is initial temperature, $I(\alpha)$ is the integral function, and $f(\alpha)$ is the solid state algebraic form of the mathematical model used to calculate activation energy. Hence from Equation (7), the kinetic parameters can estimate using the model as an integral form of the kinetics equation.

The number of integral methods for kinetics study has been derived from Equation 4. Hence, in this study, we performed iso-conversional (model-free) methods such as Kissinger Akhira Sunose (KAS), [394] Flynn Wall Ozawa (FWO), Tang, Starink, Vyazovkin and Vyazovkin AIC model used to find out kinetics parameter at particular conversion (α). The $Z(\alpha)$ master plot was used for the reaction mechanism.

4.3. Iso-conversional model (model-free)

4.3.1. Ozawa Wall Flynn (FWO) method

FWO method is derived by integral with Doyle's empirical approximation over the integral of temperature. [395] [396] Therefore, the resulting equation can be obtained in every conversion point at three heating rates.

$$\log\beta = \log\frac{AE_a}{RI_\alpha} - 2.315 - 0.457\frac{E_a}{RT} \ldots\ldots\ldots\ldots\ldots (8)$$

Hence,

From Equation (8), the experimental value can be evaluated as (-2.315 +0.457x), and a plot between log β verses 1\T capitulates the E_a/R.

4.3.2. The Kissinger Akhira Sunose (KAS) method

This differential iso-conversional method is used to predict the kinetics parameters like Arrhenius activation energy, order of reaction, and frequency factor with the relationship of heating rate; therefore, equation for KAS is as follows- [397] [398]

$$\ln\frac{\beta}{T^2} = \ln\frac{AE_a}{RI_\alpha} - \frac{E_a}{RT} \ldots\ldots\ldots\ldots\ldots\ldots\ldots\ldots (9)$$

Where β ⟶ Heating Rate.

Now,

The plot between ln β/T^2 Vs. 1/T capitulate the E_a/R at very each conversion point (α).

4.3.3. Starink method

Starink proposed the method of iso-conversion with the combination of the FWO and KAS methods. [397]

$$\ln\frac{\beta}{T_\alpha^S} = Constant - \frac{BE_a}{RT_\alpha} \ldots\ldots\ldots\ldots\ldots\ldots\ldots\ldots (10)$$

Therefore, utilizing temperature integrate approximation, the value of S and B obtained by starink is 1.92 and 1.0008. [399] so, Equation (10) can be rewritten as -

$$\ln\frac{\beta}{T^{1.92}} = Constant - 1.0008\ \frac{BE_a}{RT_\alpha} \ldots\ldots\ldots\ldots\ldots\ldots\ldots (11)$$

Hence,

From Equation (11), the plot between $\ln\frac{\beta}{T^{1.92}}$ Vs $\frac{BE_a}{RT_\alpha}$ give the linear slop of (-1.0008 $\frac{E_a}{R}$).

4.3.4. Tang method

The apparent activation energy is calculated through the Tang method[400] with the following equation.

$$\ln\frac{\beta}{T^{1.8947}} = Constant - 1.00145\ \frac{E_a}{RT_\alpha} \ldots\ldots\ldots\ldots\ldots\ldots\ldots (12)$$

Hence,

At every conversion point, the plot between $\ln\frac{\beta}{T^{1.8947}}$ Vs $\frac{E_a}{RT_\alpha}$ gives the linear relation with a slop of 1.001450 $\frac{E_a}{R}$.

4.3.5. Vyazvokin

In Vyazovkin [401] [402] methods, the iso-conversional nonlinear equation is used to calculate the more accurate activation energy. The Equation (14) for determining the activation energy at each point of conversion (α) with minimizing the particular Equation (13).

$$\Theta = \sum_i^n \sum_{j\neq i}^n \frac{J(E_\alpha T_{\alpha i})\beta_j}{J(E_\alpha T_{\alpha j})\beta_i} = min \ldots\ldots\ldots\ldots\ldots\ldots\ldots\ldots (13)$$

$$J(E_\alpha T_\alpha) = \int_0^{T_\alpha} Exp\left(\frac{E}{RT}\right) dt \ldots\ldots\ldots\ldots\ldots\ldots\ldots (14)$$

Putting the experimental data of T and β in Equation (13) and minimizing the Equation (13) using Senum- yang approximation Equation.15 [403] gives the numerical value of activation energy at each conversion point (α).

$$J(E_\alpha T_\alpha) = \frac{Exp\,(-x)}{x} \cdot \frac{x^3+18x^2+86x+96}{x^4+20x^3+120x^2+240x-120} \ldots\ldots\ldots\ldots (15)$$

4.3.6. Vyazovkin AIC

Vyazvokin AIC is a modified version of the Vayzvokin method, which is also an advance iso-conversional method for avoiding the unwanted straightening of apparent activation energy vs. conversion (α) curve**.** In the modified Vyazovkin method, [404][405] the temperature integral is formulated by Trapezoidal rule approximation of definite integral Equation (16), which varies from $T_{\alpha-\Delta_\alpha}$ to T_α hence small variation in conversion leads to assuming the activation energy (E_a.).

$$J(E_\alpha T_t) = \int_{T_{\alpha-\Delta_\alpha}}^{T_\alpha} Exp\left(\frac{-E_\alpha}{RT_t}\right) dt \ldots\ldots\ldots\ldots\ldots\ldots (16)$$

$$\Theta = \sum_{i}^{n} \sum_{j\neq 1}^{n} \frac{J(E_\alpha T_i(t_\alpha))}{J(E_\alpha T_j(t_\alpha))} = min \ldots\ldots\ldots\ldots\ldots\ldots\ldots (17)$$

From Equation (17), T (t) where t = 1, 2, 3……n is a variation of temperature and minimum value of function varying per activation energy (E_a).

4.4 Interpretation of Pre exponential kinetic factor and Thermodynamic barriers of random nucleation in Gd_2O_3 NCs

The iso-conversional model in earlier section 4.3 was used to calculate the apparent activation energy at each conversion point (α). However, the pre-exponential kinetics factor cannot be reliable using the above iso-conversional models, [406] hence the pre-exponential kinetic factor can interpret using the modified Kissinger method Equation (18)

$$\ln\left(\frac{\beta}{T_p^2}\right) = -\frac{E}{RT_p} + ln\left(\frac{AR}{E}\right) \ldots\ldots\ldots\ldots 18$$

Where T_p = Peak temperature from DTG curve at all heating rates.

As we know, the KAS model is used at a different heating rate, and it gives the single value of apparent activation energy for all conversion points (α), which cannot be suitable to estimate the pre-exponential factor; hence the activation energy calculated from Vyazovkin AIC was used to estimate the pre-exponential kinetic factor.

$$A_\alpha = \frac{\beta\, E_\alpha exp\left(\frac{E_a}{RT_p}\right)}{RT_p^2} \ldots\ldots\ldots\ldots\ldots\ldots 19$$

Where, A_α = is a pre-exponential kinetic factor at each conversion point (α).

Now, after the calculation of activation energy and pre-exponential kinetic factor at each conversion point, the thermodynamic barriers like ΔG (difference in Gibbs free energy), ΔS (difference in entropy), and ΔH (difference in enthalpy) were interpreted using the Equation 20, 21, 22. [399,407]

$$A_\alpha = \beta\, E_\alpha exp\left(\frac{E_\alpha}{RT_p}\right)\text{.....20}$$

$$\Delta G = E_\alpha + RT_p in\left(\frac{K_b T_p}{hA}\right)\text{.....21}$$

$$\Delta S = \left(\frac{\Delta H - \Delta G}{T_p}\right)\text{.....22}$$

$$\Delta H = E_\alpha - RT_\alpha\text{.....23}$$

Where K_b = Boltzmann constant ($1.381 \times 10^{-23} JK^{-1}$), T_p = Peak temperature in Kelvin (K) from DTG curve, h = planck constant ($6.63 \times 10^{-34} m^2 kgs^{-1}$). ΔG is the difference of available free energy at peak temperature to drive. ΔS is the randomness of the system at a peak temperature, and ΔH suggests the difference in energy during the preparation of Gd_2O_3 nanoclusters.

4.5 Interpretation of nucleation rate as a function of Interfacial energy, Thermodynamic and Kinetic factors

The nucleation rate for prepared Gd_2O_3 nanoclusters can be estimated by Equation (24), given below. [408]

$$J_n = J_k exp\left(\frac{-\Delta G}{RT}\right) = Aexp\left(\frac{-E_a}{RT}\right) exp\left(\frac{-\Delta G}{RT}\right)\text{.....24}$$

Where J_n = Nucleation rate of nuclei in $\mu m^{-2}/min^{-1}$, J_k = nucleation reaction kinetics of the system $\left(Aexp\left(\frac{-E_a}{RT}\right)\right)$, R = Universal gas constant (R = 8.314 J/mol. K), ΔG = thermodynamic energy barriers to initiate the nucleation and T = Temperature in kelvin (K). [372,409,410]

Thermodynamic parameter (Q) is expressed by Equation 25, which is directly proportional to interfacial energy (Υ) and molecular volume (V_m) of the nanocluster. ($V_m = M/\rho_{nm} N_A$,

where M is molar mass, ρ_{nm} is the density of nanoclusters, and N_A is Avogadro number) and inversely proportional to temperature (T) and Boltzmann constant (k_B). [411]

$$Q = \frac{16\pi V_m^2 \gamma^3}{3(k_B T)^3} \ldots\ldots\ldots\ldots\ldots\ldots 25$$

Where thermodynamic parameter Q *is express by* $\left(\frac{\Delta G}{RT}\right)$ and the interfacial energy can be calculated by putting the value of Q in Equation (25).

4.6 Experimental sections

4.6.1 Chemicals Used

Analytic high-grade gadolinium nitrate hexahydrate salt (99% of purity) ($Gd(NO_3)_3.6H_2O$) and Pure L –Ascorbic acid was purchased from Sigma Aldrich used during the experiment; Bovine serum albumin (BSA) purchased from SRL. Ultrapure deionized water was used throughout the experiment. All the above chemicals were used without any adulteration and further purification.

4.6.2 Synthesis of Gd_2O_3 NCs

Before starting the experiments, aqua regia ($3HNO_3$:1HCL) was used to thoroughly wash the glassware with further rinsing with ultrapure water (DI water). In the optimized synthesis procedure, the gadolinium nitrate hexahydrate salt (5 mM) was dissolved in 10 ml di water in the 150 ml borosil conical flask, followed by adding L-ascorbic acid (20 mg/ml) into the solution dropwise and keeping this solution on 55 °C/min set hot plate at 900 rpm. After 5 min of stirring, bovine albumin serum albumin (450 mg/ml) was added to the solution and stirred for 2 hrs. Afterward, the solution was further incubated for 72 hrs in the incubator, and the solution color changed from colorless to light yellow, indicating the formation of new gadolinium oxide nanoclusters. During the complete course of the reaction procedure, the reacting system was tightly sealed to avoid contamination and

oxidation of the solution. Finally, the prepared Gd_2O_3 nanocluster solution was centrifuged at 15000 rpm for 5 minutes to separate unreacted ligands and bigger particles.

4.7 Characterization

Fabricated gadolinium oxide nanoclusters (Gd_2O_3 NCs) were characterized using microscopic and spectroscopic techniques. The UV Vis spectroscopy (Elico SL210 spectrophotometer) was used to record nanoclusters' absorbance. The Thermogravimetric analysis (TGA) was performed using STA 6000 PerkinElmer (Singapore) at different heating rates of 10 °C/min, 15 °C/min, and 20 °C/min. The Crystallinity and phase of nanoclusters were examined using a powder XRD instrument (Brucker model –D8 Advance (Eco)). The size and morphology of nanoclusters were investigated using high-resolution Transmission electron Microscopy (HR –TEM) (FEI Tecnai G220 Twin) with 200 kV electron beam voltage. The FTIR analysis of gadolinium oxide nanoclusters were perfumed using an FT-IR spectrometer (model Nicolet iS5) at KBr pellets in the 4K to 400 cm^{-1} range. The XPS spectrum analysis using X-Ray photoelectron spectroscopy (model PHI 5000 Versa Probe III).

4.8 Result and discussion

The size and morphology analysis of Gd_2O_3 nanoclusters was performed using the 10-times diluted Gd2O3 NCs on the TEM grid. Further spectroscopic characterization like FTIR, XPS, XRD, and TGA was performed using vacuum-dried Gd_2O_3 nanoclusters.

4.8.1 UV-VIS Spectroscopy

UV-Vis spectra of prepared nanoclusters and bovine serum albumin (BSA) were observed with a characteristic peak at 266 nm and 280 nm (due to the disulfide bond of aromatic residue), [346] respectively, in Figure 4.1(a). The hyperchromic shift of 14 nm concerning BSA protein gave the concept of change in the electronic environment around the different

amide bonds during the formation of gadolinium oxide nanoclusters. [347] Additionally, the absence of any spectral peak on the entire range of visible spectra (400 nm - 800 nm) gave conclusive evidence of the formation of ultra-fine gadolinium oxide nanoclusters. [344] [412]

4.8.2 Infrared Spectroscopy and Surface analysis

Infrared spectroscopy spectra of BSA-protected gadolinium nanocluster and bovine serum albumin (BSA) are displayed in Figure 4.1(b). The characteristic band of BSA protein absorbed for amide II (1490 cm^{-1} - 1570 cm^{-1}), and amide I (1613 cm^{-1} - 1690 cm^{-1}) coincide with N-H bending and C = O stretching, respectively. [361] [412] The change in intensity of amide II and amide I spectra of nanocluster concerning BSA protein announce the interaction of gadolinium salt with the N –H and C=O protein moiety. These reductions in the intensity of nanoclusters in the amide I are due to the reduction of the α – helix of BSA protein. [364] The spectral shift of the nanocluster of ~1 nm (1654 cm^{-1} -1653 cm^{-1}) in amide A concerning the BSA (moiety –CN & N-H) is well exposed. However, the nanocluster's C = O stretching bond is significantly reduced compared to BSA protein spectra (3442 cm^{-1}-3437 cm^{-1}), revealing the encapsulation of BSA over prepared gadolinium oxide NCs. [152] The chemical composition through the XPS spectrum of prepared BSA templated gadolinium oxide nanoclusters recorded the peak at 143.3 eV, which corresponds to Gd ($4d^{5/2}$) Figure 4.2 (a) spin-orbital peaks. [413] The C (1s) spectrum of nanoclusters shows (Figure 4.2 (b)) three characteristic peaks of 284.5 eV, 285.7 eV, and 287.6 eV correspond to mono oxygenated carbon, C-O, and the existence of carbonyl and hemiketal groups respectively. [414] [415] The deconvoluted spectral peak of O (1s) shows two distinct peaks of 531.1 eV and 532.2 eV, which correspond to surface adsorbed oxygen [416] and –C-O-bond. [417] Figure 4.2 (c)

4.8.3 Size and phase analysis

The size and morphology of BSA templated gadolinium oxide nanoclusters are characterized by high-resolution transmission electron microscopy (HR-TEM) and displayed in the microscopic image in Figure 4.3(a). The average diameter of prepared nanoclusters was 0.86 ± 0.29 nm, which is ultra-fine in size. Histogram plot and Gaussian distribution (Inset: Figure 4.3(a)) of prepared nanoclusters were determined by utilizing approximately 270 data points from the acquired TEM image

(a) **(b)**

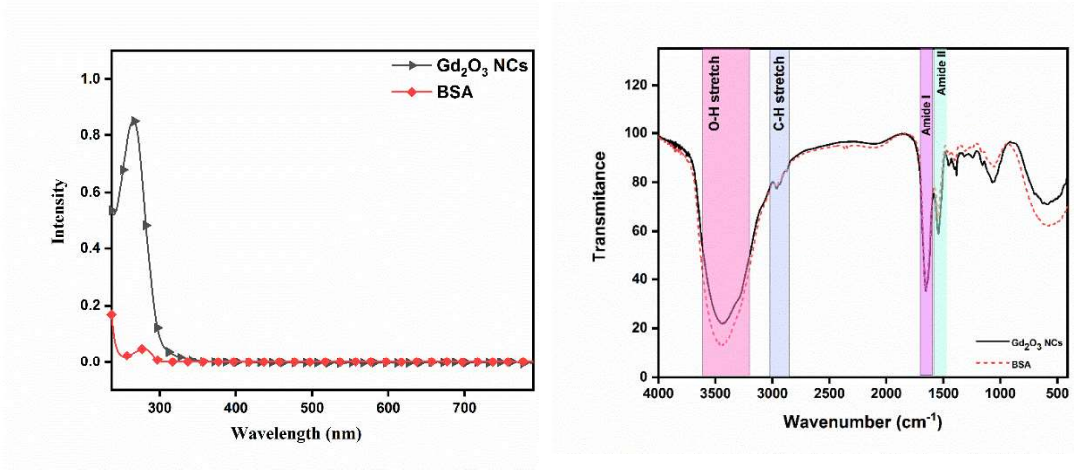

Figure 4.1: (a) UV-Vis spectroscopy spectrum of Gd_2O_3 nanoclusters and BSA protein. (b) Fourier transform infrared spectroscopy (FTIR) spectra for Gd_2O_3 nanoclusters and BSA protein.

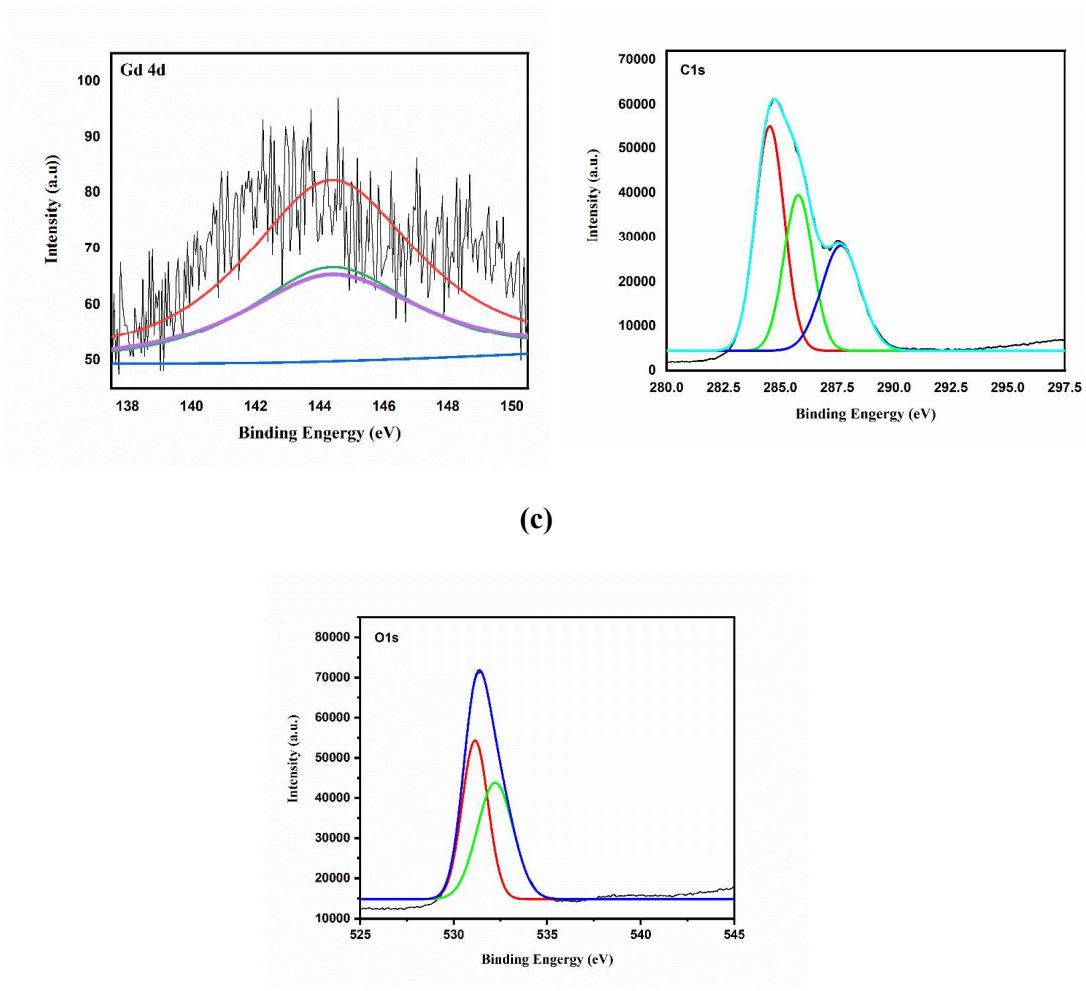

Figure 4.2: Full X-ray photoelectron spectroscopy (XPS) spectra of (a) Gd 4d, (b) C1s, and (c) O1s for prepared Gd_2O_3 nanoclusters.

Furthermore, the phase and crystallinity of prepared nanoclusters were thoroughly investigated using powder X-ray diffraction analysis (Figure 4.3 (b)). The XRD pattern of BSA templated nanoclusters did not show any characteristic peak, which strongly supports the theory of encapsulation of BSA over the prepared gadolinium oxide nanoclusters. [325,344]

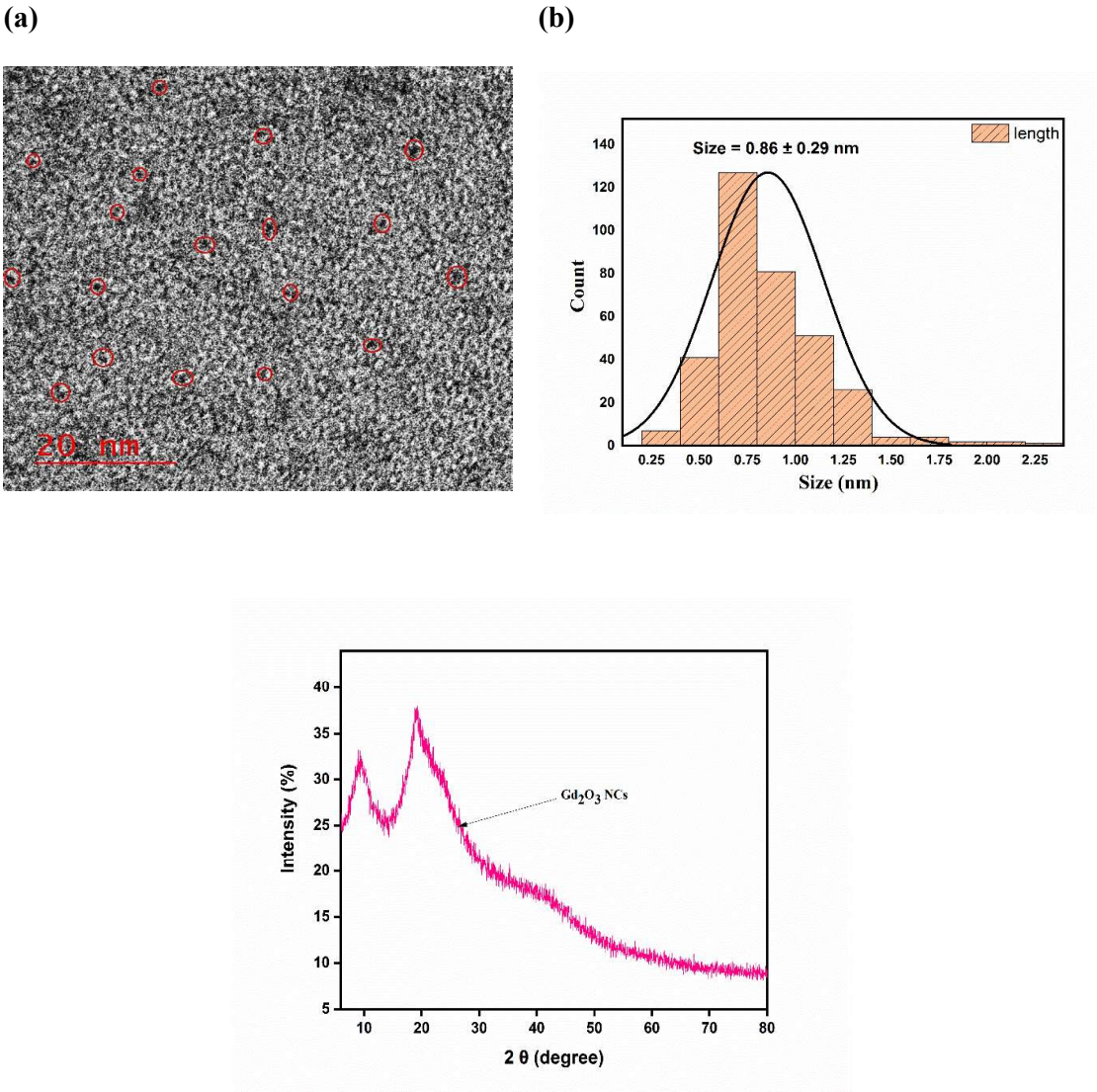

Figure 4.3: (a) High-resolution Transmission electron microscopy (HR- TEM) spectrum for Gd_2O_3 nanocluster, (b) Histogram distribution for selected image with average diameter of 0.86 ± 0.29 nm. (c) HR-XRD for prepared Gd_2O_3 nanoclusters with amorphous in nature.

.

4.8.4 Determination of Reaction kinetics model and pathways

A direct model based on differential and integral approaches has been carried out to predict the reaction mechanism as a function of conversion (α). This study used a *Z-master* plot [394] based on the p (u) method to predict the solid-state conversion. Experimentally calculated data at specific conversion points are compared and plotted against the

theoretical models to understand the reaction kinetics. The list of different forms of function [$I(\alpha), f(\alpha)$] represents in Appendix Table A4.

The $Z(\alpha)$ master plot, i.e., an integral part and differential function at 10 °C/min, 15 °C/min, and 20 °C/min, is shown in Figure 4.4 (a). Based on the comparative data of experimental and theoretical $Z(\alpha)$ master plot curves, it was observed that the reaction model depends upon the reaction progression. The $Z(\alpha)$master plots for different solid-state reaction models are abbreviated by Khawam [418] and achieved by plotting $\frac{f(\alpha)\times I(\alpha)}{f(0.5)\times I(0.5)}$ as a function of each conversion (α), where $\alpha = 0.5$ is taken as a reference point.

Hence

$$z(\alpha) = \frac{f(\alpha)\times I(\alpha)}{f(0.5)\times I(0.5)} = \left(\frac{T_\alpha}{T_{0.5}}\right)^2 \times \frac{(d\alpha/dt)\alpha}{(d\alpha/dt)0.5} \quad \text{.....26}$$

The plot $\frac{f(\alpha)\times I(\alpha)}{f(0.5)\times I(0.5)}$ Vs. specific conversion point (α) at different heating rates is shown in Figure 4.4 (a). From conversion 0.05-0.2, 0.2-0.25, 0.3 and 0.4 - 0.95, the model followed are D2, D3, R2 and R3 mechanism respectively. The nature of the plot is similar to all three mentioned heating rates.

4.8.5 Estimation of apparent value of activation energy concerning reaction progression

The activation energy (E_a) is the minimum energy required to initialize any reaction. The value of activation energy of Gd_2O_3 NCs in the BSA matrix was computed using model-free iso-conversional methods (Table 4.1). The result for E_a is displayed in Figure 4.4 (b).

(a) **(b)**

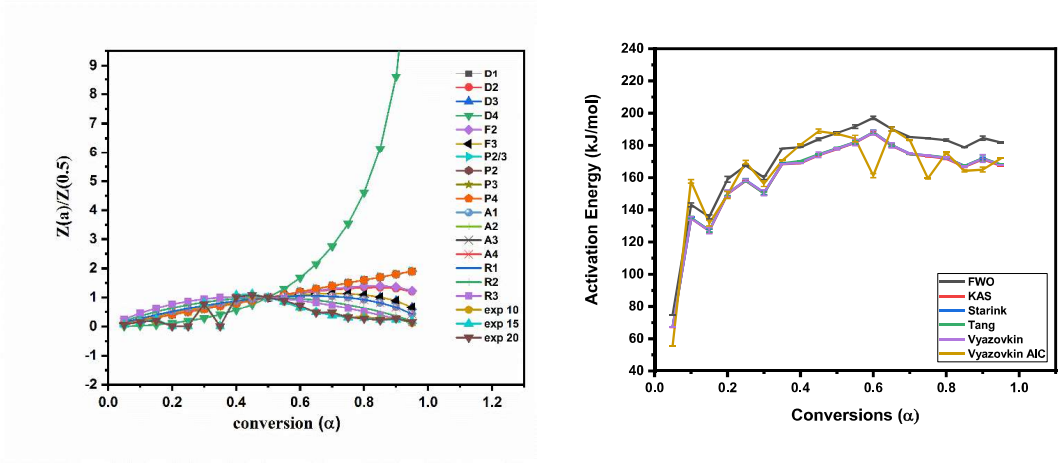

Figure 4.4: (a) *Z(α)* master plot at a different conversational point for exploring the thermal decomposition reaction mechanism at 10 °C/min, 15 °C/min, and 20 °C/min. (b) All possible apparent activation energies from an iso conversion model at all the conversion

Table 4.1: Comparative study for activation energy using different iso-conversional models

Activation Energy						
model / Conversion (α)	FWO (kJ/mol)	KAS (kJ/mol)	Starink (kJ/mol)	Tang (kJ/mol)	Vyazovkin (kJ/mol)	Vyazovkin AIC (kJ/mol)
0.05	74.86	67	67.35	67.4	67.41	55.6
0.1	143.117	134.6	135	135.11	134.6	79.15
0.15	135.6	126.8	127.16	127.27	127.08	131.7
0.2	159.0	149.86	150.24	150.35	150.1	149.26
0.25	167.47	158	158.41	158.13	158.29	169.61
0.3	159.96	150.3	150.7	150.8	150.63	156.25
0.35	178.09	168.37	168.76	168.88	168.6	170.6
0.4	178.77	168.9	169.3	170.2	169.21	180.39
0.45	183.79	173.88	174.27	174.40	174.13	188.80
0.5	187.67	177.6	178	178.10	177.90	187.10
0.55	191.68	181.56	188.1	182.10	181.82	184.28
0.6	197.98	187.7	188.1	188.26	187.97	161.26
0.65	190.24	179.77	180.19	180.32	180.04	190.23
0.7	185.25	174.5	174.9	174.5	174.79	183.15
0.75	184.46	173.32	173.7	173.91	173.64	159.52
0.8	183.29	171.7	172.24	172.38	172.12	175.52
0.85	178.76	166.6	167.16	167.32	167.07	164.20
0.9	184.52	171.39	171.9	172.08	171.83	165.03
0.95	181.81	167.36	167.94	168.12	167.89	172.02
Average	**154.28 kJ/mol**	**145.20 kJ/mol**	**145.87 kJ/mol**	**145.69 kJ/mol**	**145.48 kJ/mol**	**143.98 kJ/mol**

The apparent value of E_a at specific conversions (0.05 to 0.95) was computed as the slope of straight regression lines for mentioned models. The sinusoidal fluctuation in the value of E_a is observed as the conversion increased from 0.05 →0.95. The average calculated value of activation energy for Tang, Starink, KAS, FWO, (Figure 4.5 (a, b, c, d)) Vyazovkin and Vyazovkin AIC was found to be 145.69, 145.87, 145.20, 154.28, 145.84, and 143.98, respectively. The obtained value of activation energy is very well following the ICTAC recommendation [401] (Variation of E_a should fall around ± 5% of average E_a value). By closely monitoring the change in activation energy value with respect to specific conversion, seven significant phases were identified, which were found to simulate the reaction progression curve. In the first phase (0.05→0.25), the value of activation energy increase from 55.6→169.61, whereas in the second phase (0.25→0.3), the value of activation energy decreases (169.91→156.25), in the consecutive third (0.3→0.45), fourth (0.45→0.55), fifth (0.55→0.6), sixth (0.6→0.65) and seventh (0.65→0.95) phase the observed sinusoidal pattern of activation energy is ranging from 156.25→188.8 kJ/mol, 188.8→187.1 kJ/mol, 184.28→161.26 kJ/mol, 161.26→190.23 kJ/mol, and 190.23→172.02 kJ/mol. In a sinusoidal pattern, an increment in the value of activation energy is mainly due to the formation of stable nuclei during the process of random nucleation comply with the evolution of heat, i.e., exothermic process, while a decrease in the value of activation energy with reaction progression is due to the endothermic process. Additionally, the value of activation energy obtained from different iso-conversional methods is plotted against conversion points (0.05 to 0.95) and acquired overlapped value of E_a with reaction progression. Moreover, activation energy obtained from the Vyazovkin AIC method is further utilized to obtain kinetic and thermodynamic factors due to its efficacy and less systematic error than other iso-conversional methods.

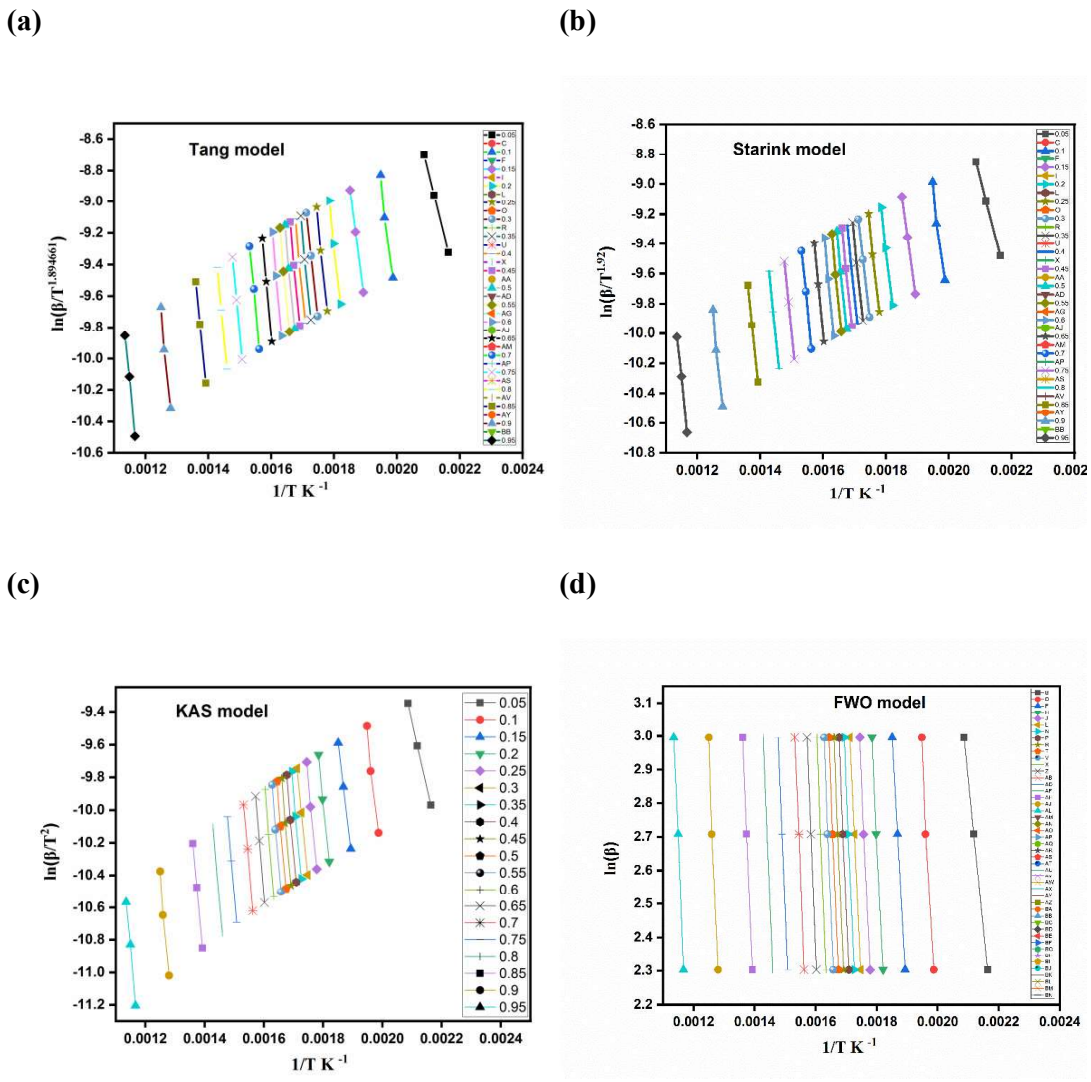

Figure 4.5: Kinetic analysis of prepared Gd_2O_3 nanoclusters using an iso conversational model. (a) Tang, (b) Starink,(c) KAS.(d) FWO.

4.8.6 Interrogation of TGA/DTG curve

DTG and TGA curves for BSA capped Gd_2O_3 nanoclusters are shown in Figure 4.6 (a, b, c) at 10, 15, and 20 °C/min heating rates, respectively. A similar trend in the TGA curve insight into the independent behavior of reaction mechanism overheating rates. With the help of analyzed data of the DTG curve, we stipulate that as the heating rate increase from

10 →15→20 ºC/min, the right shift in peak temperature (T_p) with respect to maximum mass loss rate observed and subsequently mass loss rate increased from 70% to 71%. Thus, it is clear that on increment in heating rate, the mass loss rate is also increased, probably due to the heterogeneously complex structure of BSA capped Gd_2O_3 nanoclusters. Additionally, increment in mass and heat transfer driving force increases as the heating rate escalates, leading toward the termination of overall resistance inside the Gd_2O_3 matrix, accelerating the mass loss. [419]

4.8.7 Calculation of Pre-exponential factor (A_a) as a function of conversion

Using KAS derived equation discussed earlier in section 4.3, the pre-exponential factor (A_a) was calculated in each conversion point and shown in Figure 4.6 (d). The broad range variation in the value of the pre-exponential factor suggested the heterogeneity and complexity in the BSA matrix. With the help of earlier published reports, we conclude that the lower value of the pre-exponential factor ($A_a < 10^9$ s^{-1}) indicated the lesser reactivity of the system and surface governed nucleation process, whereas, on the contrary, the high value of the pre-exponential factor ($A_a > 10^9$ s^{-1}) indicate high reactivity of system and core and surface governed nucleation process in nanoclusters. [406,420]

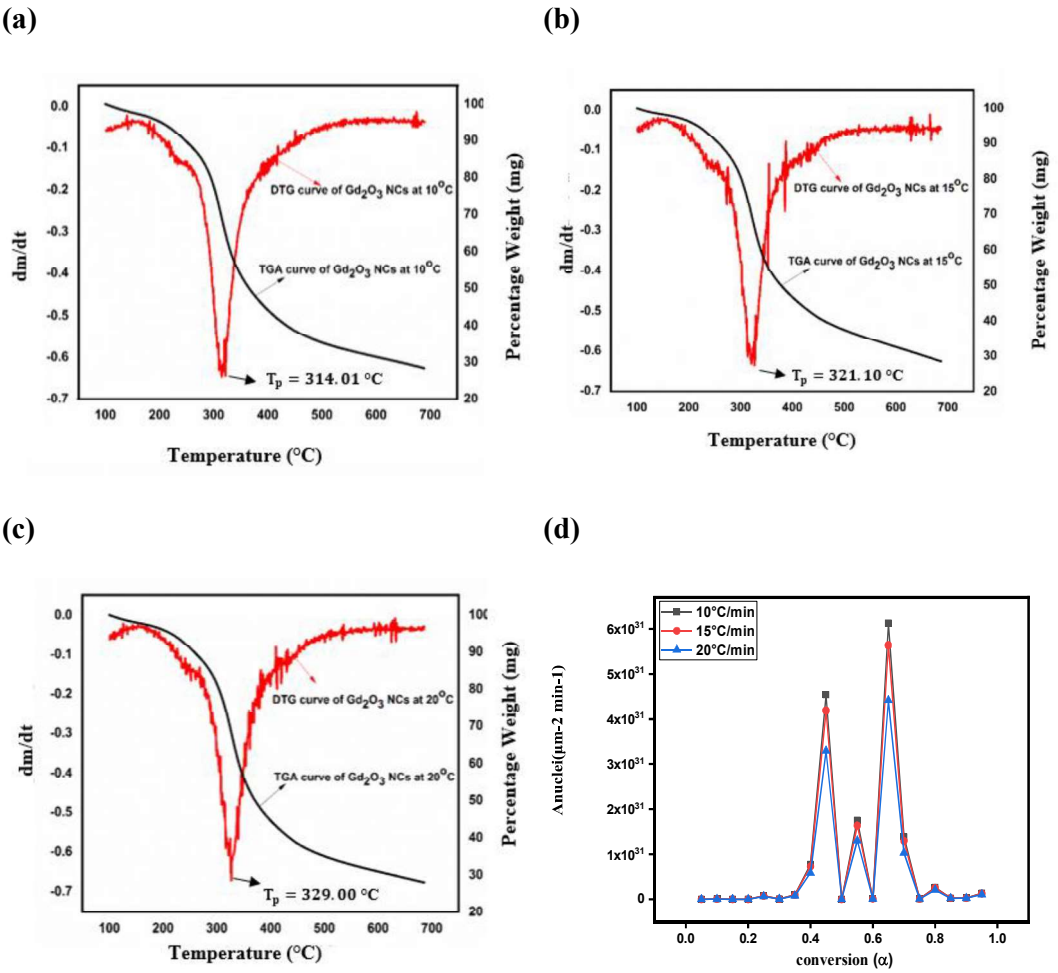

Figure 4.6: Differential thermogravimetry (DTG) and Thermogravimetry (TGA) curves of prepared Gd_2O_3 nanoclusters at (a)10 °C/min, (b) 15 °C/min,(c) 20 °C/min. (d) Pre-exponential factor for each iso conversion at 10°C/min, 15°C/min, and 20°C/min.

4.8.8 Computation of Thermodynamic parameters for reaction progression

The thermodynamic parameter was computed by utilizing equations (21) to equation (23) based on the apparent value of activation energy obtained from the Vyazovkin AIC method at all three mentioned heating rates, and the calculated values are represented in Table (4.2). The enthalpy of Gd_2O_3 nanoclusters in the BSA matrix varies from 155.61 to 164.89

kJ/mol, 153.55 to 164.78 kJ/mol, and 158.52 to 164.69 kJ/mol at 10, 15, and 20 ºC/min heating rates, respectively. Furthermore, the positive value of enthalpy suggests the endothermic nature of the reaction process. Additionally, the obtained value suggests a minimal effect of heating rate on enthalpy. At the beginning of the reaction, the value of ΔH is minimal due to the removal of moisture content. The ΔH during thermal degradation indicates the energy difference between Gd_2O_3 NCs in the BSA matrix and the formed activated complex matching with activation energy (E_a) slightly. Figure 4.7(a) Hence, the lower difference between the value of ΔH and E_a indicates the feasibility of reaction progression with the formation of the activated complex during the thermal degradation process[421].

The change in the value of Gibbs free energy (ΔG) suggested the increase in energy of a reacting system as a result of activated complex formation. [399] The variation of ΔG with respect to conversion points at different heating rates is displayed in Figure 4.7(b). The average value of ΔG at 10, 15, and 20 ºC/min heating rates is 148.38 kJ/mol, 148.39 kJ/mol, and 148.9 7 kJ/mol, respectively. The positive value of Gibbs free energy suggests the energy requirement from an external source for initiating nuclei/ activated complex formation. The change in Gibbs free energy (ΔG) is the available energy required through which the maximum amount of mechanical work can be produced for nucleation to occur. The variation in Gibbs free energy corresponds to the variation in the system accessible energy during the nucleation progresses. [422] In order for work to be done, there must be an increase in available energy, as explained in the definition of ΔG. Therefore, when the available energy increases with heating rate, ΔG also increases accordingly. Hence, the increase in ΔG with heating rate can be attributed to the increase in available energy that results from the increase in work done. indicates the high energy consumption at a high heating rate. [423] [421]

(a)

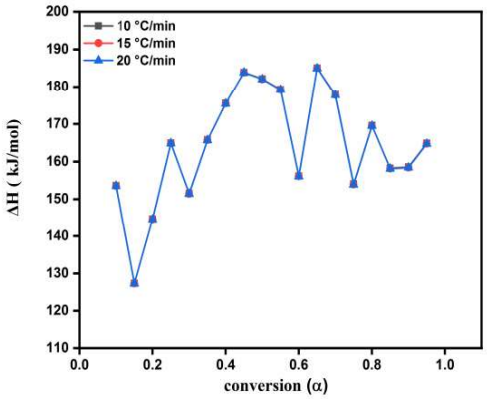

(b)

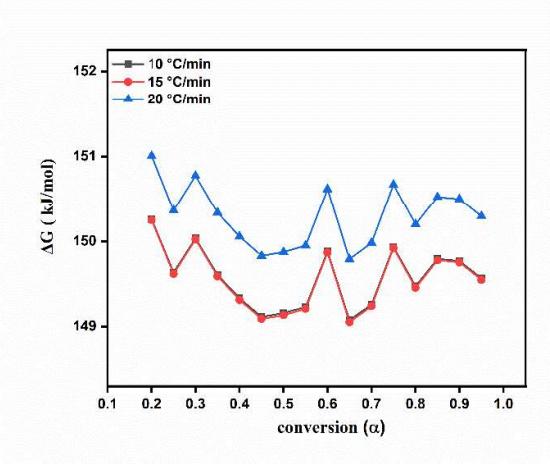

(c)

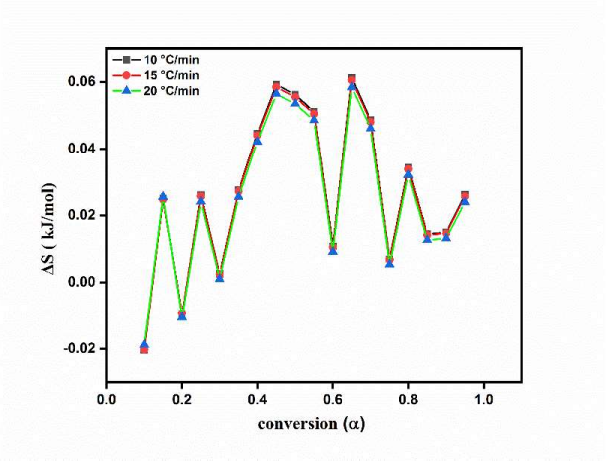

Figure 4.7: (a) Plot between enthalpy against conversion at 10 °C/min, 15 °C/min, and 20 °C/min, (b) Plot between Gibbs free energy against conversion at 10 °C/min, 15 °C/min, and 20 °C/min, (c) Plot between Entropy against conversion at 10 °C/min, 15 °C/min, and 20 °C/min.

Conversions(α)	Heating rate (10 °C/min)				Heating rate (15 °C/min)				Heating rate (20 °C/min)			
	ΔH (kJ mol^{-1})	ΔG (kJ mol^{-1})	ΔS (kJ mol^{-1})	A (S^{-1})	ΔH (kJ mol^{-1})	ΔG (kJ mol^{-1})	ΔS (kJ mol^{-1})	A (S^{-1})	ΔH (kJ mol^{-1})	ΔG (kJ mol^{-1})	ΔS (kJ mol^{-1})	A (S^{-1})
0.1	153.611	165.6027	0.02044	6.06412E+13	153.5534	165.616	0.02030	6.03749E+13	153.5276	164.1085	0.01883	5.15526E+13
0.15	127.356	112.6262	0.002509	2.43484E+11	127.2972	112.6288	0.024690	2.58357E+11	127.2549	111.8632	0.025566	2.36413E+11
0.2	144.702	150.2584	0.00946	9.99855E+12	144.6448	150.2488	0.00943	1.01644E+13	144.6108	151.0048	0.01062	8.87794E+12
0.25	164.938	149.6348	0.026071	7.34155E+14	164.8807	149.6173	0.025692	7.1011E+14	164.8477	150.3653	0.024057	5.87603E+14
0.3	151.499	150.0351	0.002495	4.38179E+13	151.4417	150.0224	0.002389	4.37898E+13	151.3998	150.7758	0.010362	3.75442E+13
0.35	165.793	149.6063	0.027576	9.05653E+14	165.7357	149.5884	0.027180	8.7386E+14	165.7022	150.3360	0.025525	7.21193E+14
0.4	175.526	149.3342	0.044619	7.10641E+15	175.4675	149.3130	0.044023	6.69487E+15	175.4334	150.0570	0.042154	5.3835E+15
0.45	183.892	149.1116	0.059250	4.17226E+16	183.8331	149.0878	0.058484	3.85058E+16	183.8003	149.8288	0.056431	3.02787E+16
0.5	182.139	149.1558	0.056190	2.91731E+16	182.0820	149.1325	0.055461	2.70361E+16	182.0479	149.8741	0.053445	2.1356E+16
0.55	179.271	149.2299	0.051177	1.61263E+16	179.2128	149.2075	0.050505	1.50484E+16	179.1796	149.9501	0.048554	1.19762E+16
0.6	156.171	149.8812	0.010716	1.26103E+14	156.1142	149.8667	0.010516	1.24489E+14	156.0804	150.6180	0.009074	1.05324E+14
0.65	185.048	149.0748	0.061283	5.63627E+16	184.9906	149.0505	0.060495	5.18354E+16	184.9486	149.7910	0.058401	4.06057E+16
0.7	177.836	149.2598	0.048682	1.27227E+16	177.7782	149.2378	0.048040	1.19051E+16	177.7281	149.9808	0.046092	9.50302E+15
0.75	154.006	149.4737	0.006937	8.72958E+13	153.9397	149.9203	0.006765	8.65465E+13	153.8898	150.6724	0.005345	7.35621E+13
0.8	169.611	149.7929	0.034306	2.43733E+15	169.5366	149.4542	0.033803	2.3249E+15	169.4866	150.2000	0.032038	1.89492E+15
0.85	158.235	149.7684	0.014382	2.34727E+14	158.1515	149.7773	0.014096	2.30061E+14	158.0940	150.5275	0.012569	1.93126E+14
0.9	158.538	149.5661	0.014940	2.79471E+14	158.7848	149.7525	0.014606	2.73362E+14	158.3803	150.5023	0.013086	2.28972E+14
0.95	164.893	149.5661	0.026110	1.21927E+15	164.7848	149.5477	0.025647	1.17242E+15	164.6935	150.2948	0.023918	9.63969E+14
Average -	**164.059**	**148.3881**	**0.02540**	**9.9.408E+15**	**164.0127**	**148.3927**	**0.026259**	**8.71867E+15**	**163.9503**	**148.9726**	**0.025398**	**6.88722E+15**

Table 4.2: Thermodynamic parameters at different heating rates with correspond to each conversion points

The value of change in entropy (ΔS) suggested the randomness [407] of the reacting system, and its variation with conversion points is displayed in Figure 4.7(c). The average value of ΔS at 10, 15, and 20 ºC/min are found to be and, respectively. The sinusoidal trend in the ΔS vs. The conversions (α) graph demonstrates the higher and lower reactivity of the system at those conversion points. After summarizing all analyzed thermodynamic results, it can be interpreted that the system's reactivity goes up and down during the entire course of reaction progression, but the net effect suggests a loss in the system's reactivity. It is necessary to mention that in the interim of reaction, the constant heat gradually provided into the system without any interruption led to escalating the free energy of the reacting system.

4.8.9 Variation in rate of nucleation concerning conversion and temperature

Due to an inadequate understanding of nanomaterials' kinetic and thermodynamic parameters, the computation of nucleation rate is complex and debatable. In previous reports, the nucleation rate is calculated by utilizing equation (24), but the kinetic term (J_k) was assumed to be constant due to assuming less importance of the J_k term as compared to interfacial energy described in the thermodynamic term. [424,425] Besides this, high-temperature analysis of nucleation rate is still lacking. Several studies demonstrate the 10-fold variation in the value of nucleation rate due to constant J_k term even at an average temperature. [426] Hence, calculating the J_k term is crucial for precisely estimating the nucleation rate at high temperatures. [427]

Consequently, the apparent value of activation energy (E_a) and pre-exponential factor (A_a) is precisely computed by the Vyazovkin AIC method and KAS-derived equation and further utilized to calculate the value of J_k. Interestingly, nucleation geometry is the essential parameter for nucleation rate and pre-exponential kinetic factor (A_a)

determination. [372] Hence, the value of A_a was changed in terms of nuclei geometry. Furthermore, the graph of nucleation rate vs. temperature Figure 4.8(a) revealed an increasing trend in the value of nucleation rates at all three heating rates. (Appendix-Table A2) For a better understanding of nucleation rate dependency on specific temperature and conversion points, a theoretical model was deduced by applying fitted experimental data. With the help of obtained data from the nucleation rate and specific temperature graph, a best-fitted exponential model $J = J_O + A_1 exp\left(\frac{(x-x_o)}{t_1}\right)$ was deduced, where A_1 and t_1 designated as exponential function constants, and their values at 10, 15, and 20 °C/min are shown in Appendix-Table A(2.1). However, the graph of nucleation rate Vs. Conversion Figure 4.8(b) points to an exponential model $J = J_O + A_1 exp\left(\frac{(x-x_o)}{t_1}\right) + A_2 exp\left(\frac{(x-x_o)}{t_2}\right)$ was found most suitable and where A_1, A_2, t_1 and t_2 are termed as exponential function constant, and their value at 10, 15, and 20 ºC/min are displayed in Appendix-Table A(2.2). Interestingly, our obtained trend in nucleation vs. temperature and conversion graphs harmonizes with previously published reports. Additionally, the nucleation rate was also calculated at 10, 15, and 20 ºC/min and found an increase in the value of the nucleation rate with a rise in the heating rate. This phenomenon is probably due to a decrease in heat and mass resistance barrier, [44] which resultant a high nucleation rate. This phenomenon is noticeable in above mentioned TGA/DTG curve Figure 4.6 (a, b, c).

4.8.10 Variation in interfacial energy with respect to conversion and temperature

Computation of interfacial energy of BSA scaffolded Gd_2O_3 nanoclusters is an essential asset for estimating several crucial physical quantities. [428] Several techniques have been used to estimate the value of interfacial energy. In line with this galvanic cell method, a short range (750-950 K) temperature is used for the determination of copper nanoparticles

[429] and the computation of interfacial energy of $CaCO_3$ at room temperature is 30-50 mJ/m^2. [424] However, no effort has been made to determine the interfacial energy of the Gd_2O_3 nanocluster in the BSA matrix at high temperatures. Hence, we exclusively calculate the value of interfacial energy concerning specific temperature and conversions. (Figure. 4.8(c)) In our study, we observed an increasing trend in the value of interfacial energy with a rise in temperature at all three heating rates. At 10, 15, and 20 °C/min heating rates the value of interfacial energy increases from 49.31→67.99 mJ/m^2, 49.77→68.67 mJ/m^2, 49.89→67.37 mJ/m^2, respectively (Appendix-Table A3). Our estimated value of interfacial energy is in good agreement with previously reported interfacial energy of nanomaterials. [45,424,428]

Furthermore, the obtained data of interfacial energy was found to best fit in linear model Y = a+bx as a function of temperature Figure 4.8(d), where a and b are linear function constants, and their values at 10, 15, and 20 °C/min heating rates are displayed in Appendix-Table A (3.1). Furthermore, the obtained plot between interfacial energy and conversion points suggested best suited second order polynomial model $Y=b_1x-b_2x^2+I$ at all three mentioned heating rates; here I is the intercept, and b_1 and b_2 are polynomial constant, and their values are displayed in Appendix-Table A (3.2). In this study, we concluded that the nucleation rate increases exponentially as the temperature rises due to the increase in surface energy value. [430]

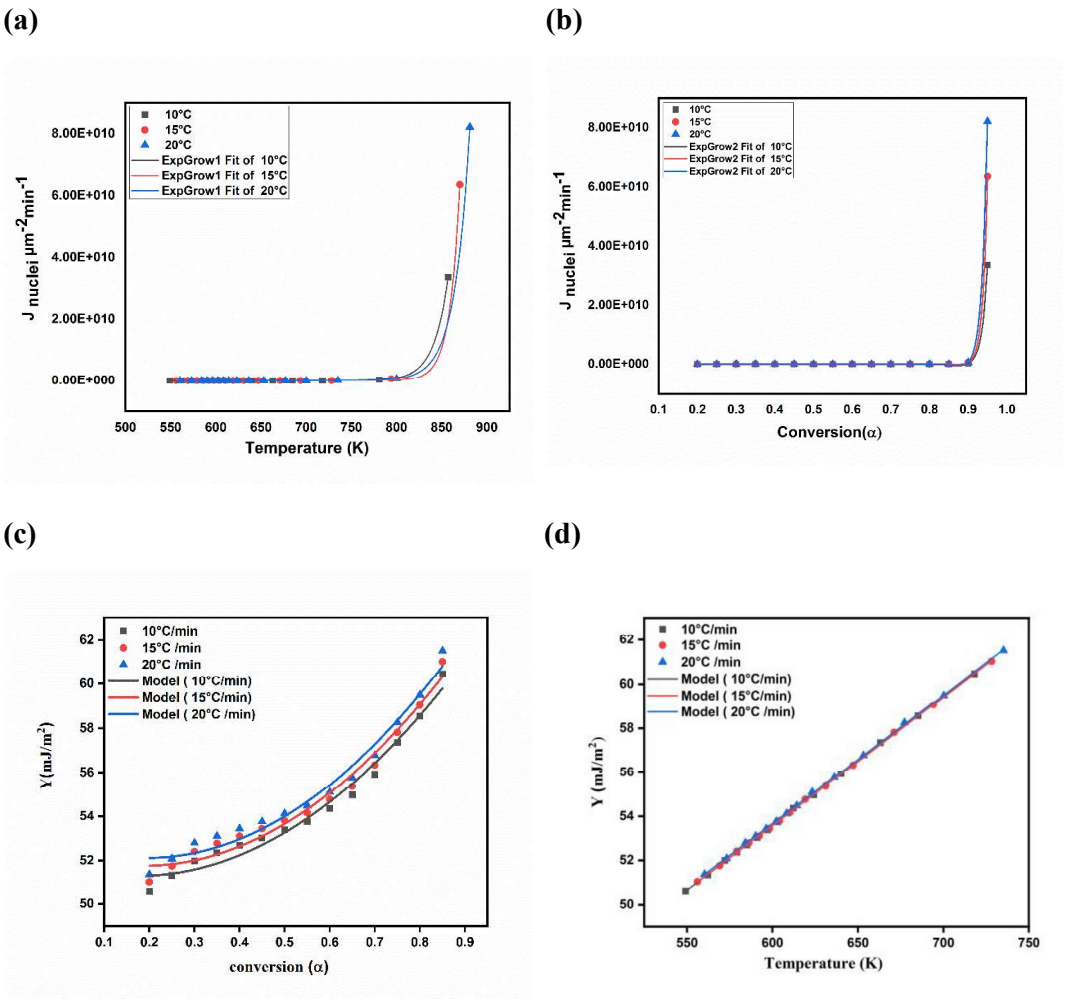

Figure 4.8: (a) Temperature dependent nucleation rate plot of Gd_2O_3 nanoclusters, (b) Conversion depnedent nucleation rate plot of Gd_2O_3 nanoclusters, (c) Conversion depnedent interfacial energy plot of Gd_2O_3 nanoclusters, (d) Temperature-dependent interfacial energy plot of Gd_2O_3 nanoclusters.